Plasma Phys. Control. Fusion 35 (1993) B205–B214. Printed in the UK

EDGE PHYSICS AND H-MODE STUDIES IN ASDEX UPGRADE

Kaufmann M., Bosch H.-S., Field A., Fußmann G., Gruber O., Herrmann A., Junker W., Kallenbach A., Köppendörfer W., Krieger K., Lackner K., Laux M., Mertens V., Napiontek B., Naujoks D., Neuhauser J., Poschenrieder W., Roth J., Ryter F., Zohm H.
Albrecht M., Alexander M., Asmussen K., Becker G., Behler K., Behringer K.[+], Bergmann A., Bessenrodt-Weberpals M., Brambilla M., Braun F., Büchl K., Carlson A., Chodura R., Cupido L.[++], de Barbieri O., de Blank H.J., de Pena Hempel S., Dorn C., Drube R., Eberhagen A., Engelhardt W., Engstler J., Fahrbach H.-U., Feist J.-H., Feneberg W., Fieg G.[†], Fuchs C., García-Rosales C., Gehre O., Gernhardt J., Götsch S., Gruber J., Günther K., Haas G., Heinemann B., Herppich G., Herrmann W., Hofmeister F., Hohenöcker H., Jacobi D., Jüttner B., Kardaun O., Kass T., Kiemer K., Kollotzek H., Kornherr M., Kurzan B., Lang P., Lang R., Lengyel L., Leuterer F., Lieder G., Manso M.E.[++], Mast K.-F., Mayer H.-M., McCarthy P.[‡]., Meisel D., Merkel R., Münich M., Murmann H., Neu G., Neu R., Noterdaeme J.-M., Pautasso G., Pitcher C.S.[*], Raupp G., Richter H., Richter T., Röhr H., Salmon N., Salzmann H., Sandmann W., Schilling H.-B., Schittenhelm M., Schneider H., Schneider R., Schneider W., Schönmann K., Schramm G., Schumacher U.[+], Schweinzer J., Scott B., Seidel U., Serra F.[++], Silva A.[++], Söldner F.X., Speth E., Stäbler A., Steuer K.-H., Streibl B., Suttrop W., Treutterer W., Troppmann M., Tsois N.[**], Ulrich M., Varela P.[++], Venus G., Vernickel H., Vollmer O., Wedler H., Weinlich M., Wenzel U., Wesner F., Wilhelm R., Wunderlich R., Zasche D., Zehrfeld H.-P.

Max-Planck-Institut für Plasmaphysik, Euratom-IPP Assoc., 85748 Garching & 10117 Berlin, Germany;
[+] Universität Stuttgart, Institut für Plasmaforschung, 70569 Stuttgart, Germany;
[++] Instituto Superior Técnico, Euratom-IST Assoc., Lisboa, Portugal;
[†] 76133 Kernforschungszentrum Karlsruhe, Germany;
[‡] University of Cork, Ireland;
[*] University of Toronto, Institute for Aerospace Studies, Ontario, Canada;
[**] Int. Research Center, Demokritos, Attiki, Greece.

1. Introduction

ASDEX Upgrade is a poloidal divertor experiment [1] very similar to ITER with respect to magnetic field properties and especially to the plasma boundary geometry. A large part of the programme on ASDEX Upgrade is therefore dedicated to investigating and optimizing reactor-relevant plasma boundary issues. ASDEX Upgrade ($R_o = 1.65\ m, a = 0.5\ m, b = 0.8\ m$) was operated with a single-null divertor configuration (SN) and in the following parameter regime: $B_T = 1$ to 2.7 T; $I_p = 0.6$ to 1.2 MA; $q_{95} = 2.1$ to 5.3; filling gas: mostly D_2 (partly He and H_2 minority); both directions of ion ∇B drift (drift to X-point: $\rightarrow \times$, opposite: $\leftarrow \times$); ohmic heating (up to 1.6 MW); ICRH H^+ minority and second harmonic (up to 2.4 MW) and recently NI (up to 5.0 MW).

0741-3335/93/000205+10$07.50

The plasma boundary was diagnosed with a wide set of diagnostics: 2 bolometers with 64 spatial channels, 3 bremsstrahlung detection systems with 82 spatial channels, 8 CCD cameras at different poloidal and toroidal positions, a DCN laser interferometer with 8 lines of sight, diode arrays equipped with D_α filters for the divertor region and the inner heat shield, flush-mounted Langmuir probes in the target plates, a movable Langmuir probe in front of the outer target plate, a mass spectrometer measuring the exhaust in a pumping port, neutral gas gauges throughout the vessel, a radiometer measuring T_e in the outer scrape-off layer in the mid-plane, a 2-channel reflectometer, a spectrometer observing the inner heat shield with 10 spatial channels, a divertor spectrometer with 16 tangential lines of sight, and a boundary layer spectrometer with lines of sight approximately perpendicular to the outer target plate, and a thermography camera for both the inner and outer target plates.

This contribution is concerned with H-mode studies and edge physics in general. The L/H-power threshold, H-mode confinement, details of ELM dynamic and "dithering" L/H-transitions will be discussed. The edge physics investigations are concerned with model calculations and validations, the characteristic "approach" to the density limit (DL), target plate sputtering and the influence of hydrocarbons, asymmetries and drifts depending on the direction of the toroidal magnetic field, and finally first results of high-Z material experiments.

2. H-Mode in ASDEX Upgrade

ASDEX Upgrade H-mode experiments have been performed so far with three heating methods (Ohmic [20], NI and ICRH [23]), in deuterium with the $\rightarrow \times$ ion drift. There was even easy access to the H-mode with ohmic heating only, especially at low q-values. ELM free phases have been achieved in ohmic plasmas at $q_{95} \simeq 2.1$ and with NI (Fig. 1). Long-lasting stationary ELMy H-mode discharges, longer than $\simeq 10\ \tau_E$, were obtained (Fig. 1) with all three heating methods. Altogether, the H-mode was observed in deuterium with all three heating methods and for $\bar{n}_e = 0.25$ to $1.0 \cdot 10^{20}$ m^{-3}; $B_T = 1.0$ to 2.0 T; $I_p = 0.6/1.2$ MA; $q_{95} = 2.1$ to 5.3.

As in other devices [2], it is possible to represent the necessary power P_{thr} to achieve the L/H-transition as a function of $\bar{n}_e \cdot B_T$ only (see Fig. 2), independently of the heating method. Normalizing by the plasma surface area (S), as in [2], gives for ASDEX Upgrade $P_{thr}/S = 0.042\ \bar{n}_e \cdot B_T[10^{20} m^{-3} T]$, about twice lower than in [2] for comparable devices. Close to the transition a large number of characteristic "dithering cycles" was observed (see Sect. 4, in Fig. 2 marked by $\Diamond$). With ohmic and NI heating methods ELM-free periods (H*) were obtained. With NI, a sequence of cycles starting with a short 3 ms L-mode, a subsequent dithering period and an ELMy H-mode, followed by a 200 ms H* period which ended with 100 % bulk plasma radiation, were found (Fig. 1). The most striking feature of this sequence is the very short duration of the L-phase, however sufficient to reduce radiation and density back to their levels prior to the H-phase, allowing thus this regular repetition.

The energy confinement times showed enhancement factors τ_E^H/τ_E^L of 1.1 in the dithering periods, 1.6-1.8 during stationary ELMy phases and up to 2.0 in H* periods.

As usual the density and temperature profiles, already broader than on ASDEX, broadened after the L/H transition and the density profile showed a shoulder in the H* period. These well-known H-mode features are not further described here, but can be found in [20].

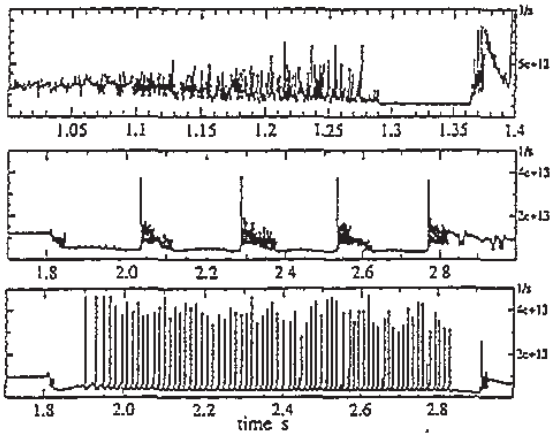

Fig. 1 D_α time traces in divertor for different H-discharges; top: ohmic H-mode with 80 ms Elm-free phase; middle: NI L/dither/ELM-free sequence; bottom: NI quasi-stationary with type I ELMs

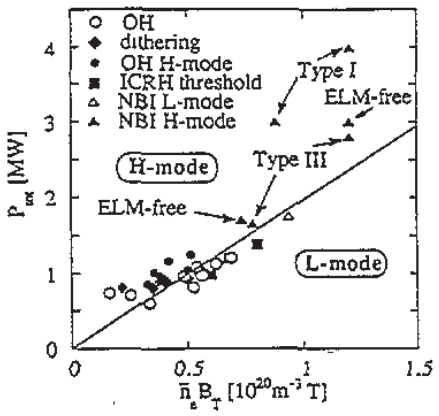

Fig. 2 H-mode power threshold: and operational window: total heating power versus $\bar{n}_e \cdot B_T$ the line indicates the power threshold

3. ELM Dynamics

The ELMs observed are of type III and type I, most easily distinguished by $d\nu_{ELM}/dP < 0$ for type III and $d\nu_{ELM}/dP > 0$ for type I. Four phases can be distinguished during one type III ELM event:
1. A coherent magnetic precursor oscillation at about 80 kHz. 2. Magnetic turbulence develops, with a fast rise of D_α and other lines in the divertor region. Figure 3 shows the intensity of D_α and a C^{III} line as a function of time and the distance to the target plates [22]. Within a time less than 10 μs D_α rises on all channels. A very pronounced fast rise is also observed on those channels intersecting with the X-point region. The first fraction of energy is conducted to the target plates within 100 μs. 3. Slower particle transfer to the target plates within 0.1 to 1 ms. 4. Magnetic turbulence has ended. The D_α signals describe the decaying recycling process. Reflectometry [3] showed very low turbulence during this phase.

The new thermographic system [4] observing the target plates with high time and spatial resolution (8 kHz, $\Delta R = 3$ mm) allowed an analysis of the energy expelled from the plasma during one ELM (see Fig. 4). So far, only type III ELMs have been analyzed. During an ICR-heated ELMy period, the following time-averaged power balance was obtained: bulk plasma radiation $P_{rad} \approx 40$ %; loss during ELMs $P_{ELM} \approx 30$ %; loss in between ELMs $P_H \approx 30$ %.

The fraction of power arising at the outer divertor P_{out} to the power to the inner divertor P_{in} is about the same during and between ELMs, $P_{out}/P_{in} \approx 2$. The peak power during an ELM is about $8 \cdot P_H$; however, it spreads over a broader area of the target plates, thus leading to a short enhancement in power density of only $\approx$ 4. These values are averaged over many ELMs; a single ELM may exceed this value by a factor of up to 2.

The interferometer density profile showed a loss of 0.5 to $2 \cdot 10^{19}$ particles ($\hat{=}$ 2-5 % of plasma content) during one ELM. In combination with the energy loss one can conclude that the major fraction of the energy has to be transported by electron thermal conduction to the target plate region. This agrees well with the fast rise of line radiation in front of the target plates indicating that T_e rises on a fast time

scale. The heat transport seems to start with ergodization close to the separatrix which especially would explain the C^{III} flash in the X-point region [5].

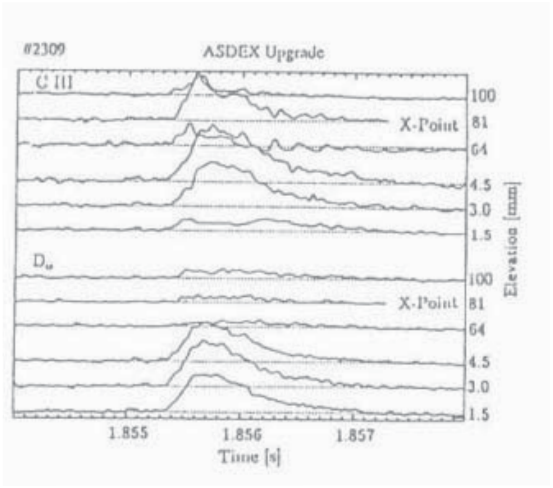

Fig. 3 D_α, C^{III} in divertor at various elevations above the target plate during an ELM event

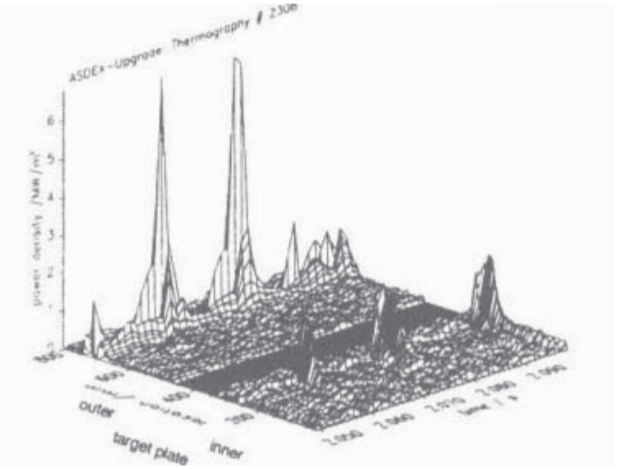

Fig. 4. Thermography of target plates during an ELMy period

4. The Dithering Cycle

Especially ohmic discharges which marginally reached the H-mode showed characteristic, mainly periodic (1 to 2 kHz) D_α-signals in the divertor (see Fig. 5) which are significantly different from ELMs and which can be identified as oscillations between L- and H-mode [5]. The number of cycles strongly depends on the rise of the heating at the transition and is a function of $d\ (P/P_{tr} - 1)/dt$.

A tentative description of the cycles assumes stabilization of the turbulence by shear rotation and a balance between the currents due to fast particle losses and those due to loss of bulk particles as a function of the electric field in the boundary [6]. The expression for the latter current scales as $j_b \propto \frac{T}{n}(\frac{1}{\lambda n} + \gamma \frac{1}{\lambda T})$. While the reduced level of turbulence reduces the decay lengths of the density λ_n and temperature λ_T and increases T, thus leading to self-stabilization of a once reached H-mode, the increase of the density n can counteract. The latter effect seems to dominate and drives the boundary back to L-mode unless a further increase of heating overcomes this dithering cycle.

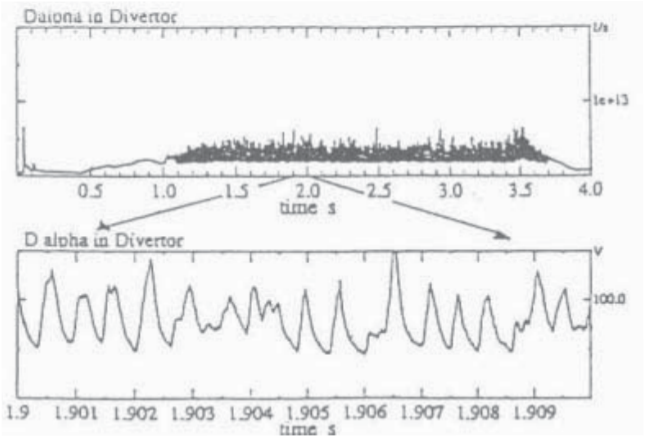

Fig. 5 D_α-signals in a dithering period

5. SOL Simulation and Model Validation

Code calculations with the B2 plasma fluid code and the EIRENE Monte-Carlo code [7] with progressively improved models simulate the scrape-off layer of ASDEX Upgrade. Comparison with experiments allows validation of different edge physics models and fitting of anomalous transport coefficients to establish a basis for extrapolation to ITER. The main experimental basis for comparison so far are the temperature and density measurements with the movable Langmuir probe [8] close to the outer divertor plate (see Fig. 6). The best agreement of the B2/EIRENE results with the data of the movable in-vessel probe data is achieved using a quite small particle diffusion coefficient $D_\perp = 0.1$ m^2/s, and $\chi_e = 1.5$ m^2/s, $\chi_i = 1.0$ m^2/s (see Fig. 7). No inward drift velocity has been used, and these transport parameters are assumed to be poloidally constant [9]. On this basis, the calculated neutral gas flux densities in the divertor agree well with the data measured by ionization gauges.

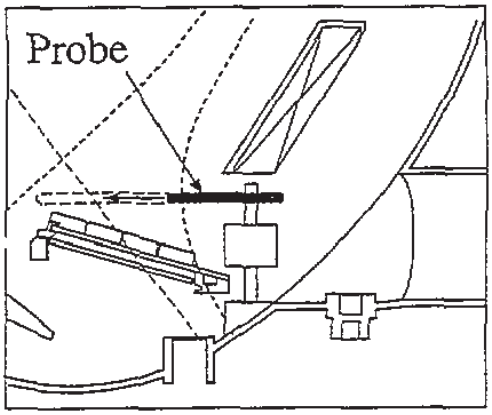

Fig. 6 Movable Langmuir probe

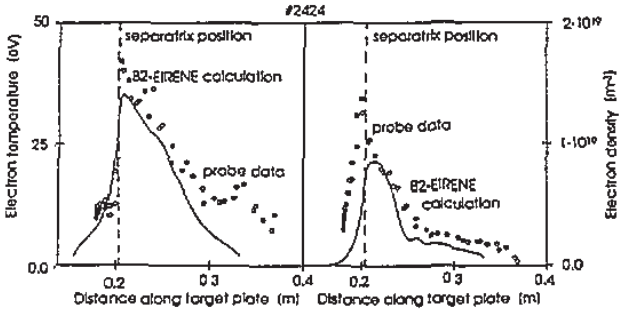

Fig. 7 Comparison of measured (circles) and calculated (lines) T_e and n_e profiles at the outer target plate

The measured n_e- and T_e-profiles in the SOL show a shoulder which extends out to the divertor baffle. Similar shoulders in n_e and T_e had already been observed in ASDEX and were attributed to enhanced turbulent transport at the outer edge region [10, 11]. In the code this outer turbulence zone has been modelled with an outward drift velocity (of 70 m/s) in the outer half of the SOL.

Only on the basis of further experimental input can it be finally decided if drift terms are needed to describe the inner part, and if the shoulder can be better modelled with a diffusion coefficient.

6. Cold Divertor, Marfes and Density Limit

One of the main goals of ASDEX Upgrade is the development of the cold divertor operation mode, which includes the need to work close to the density limit [19]. As a first step, the "typical approach" to the limit was analysed ($B_T = 1.35$ to 2.0 T, $q_{95} = 2.8$ to 5, $\rightarrow \times$, D_2). Fig. 8 shows the main elements in this approach. The density was increased with a rate, which is slow in the sense that after turnover to a density plateau only little changes can be seen. Three phases can be clearly distinguished:

Phase I: The C^{III} signal in front of the divertor plates (chord parallel to surface) indicates a divertor temperature T_d above 10 eV in agreement with Langmuir probe measurements and sputtering in the striking zone (see Sect. 7). Remarkable in this

phase is a pronounced bolometer radiation from the X-point and divertor fans of the order of 25 % of the total radiation.

Phase II: The C^{III} signal nearly disappears proving T_d to be below 5 eV, which is in agreement with measurements with built-in Langmuir probes. A target-plate Marfe seems to move in a bistable manner to the X-point. There is no pronounced change of $< Z_{eff} >$ and P_{rad}/P_{OH} when the divertor gets cold. During the end of phase II the Marfe moves upwards and can get with its front to a distance of 15 cm above the X-point. In phase II the density profile broadens, while the temperature profile steepens. The averaged $< Z_{eff} >$ stayed almost constant with a typical value of 1.7.

Phase III: At a certain q-depending position of the Marfe front and a corresponding increase of l_i the Marfe moves up and down on the high field side, and in parallel locked modes develop. This phase ends with a major current disruption. We define the density limit as the density at the beginning of phase III.

The OH density limit can be described as a Hugill limit with $\bar{n}_e = 2.8 \cdot 10^{20} m^{-2} T^{-1} \cdot B_T/(Rq_{95})$, which is a factor of 1.6 higher than in ASDEX exhibiting clearly the gain by the elongation as predicted by the Greenwald limit.

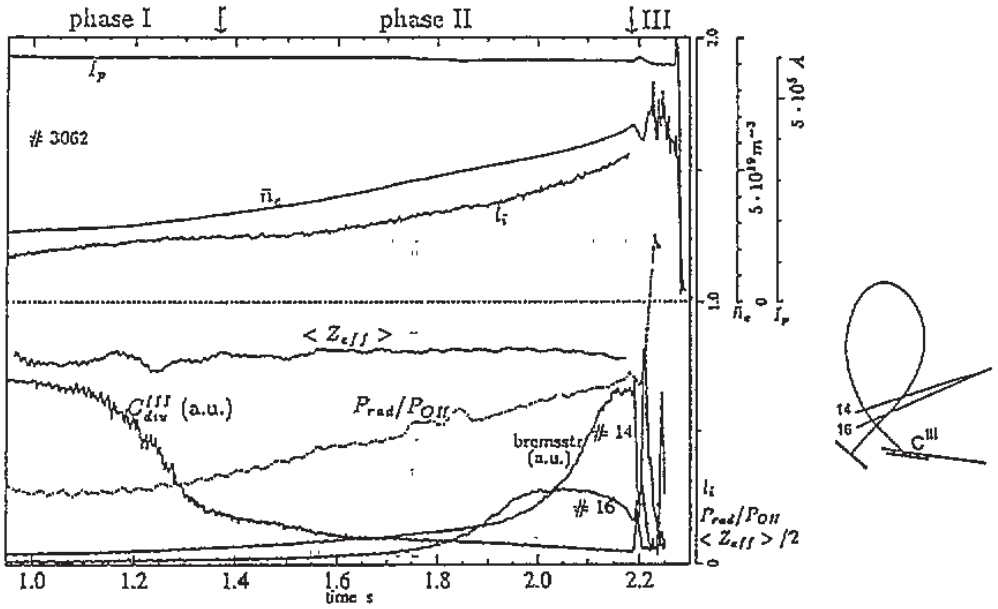

Fig. 8 A typical approach to the density limit.
The bremsstrahlung chords # 14 and #16 exhibit the smooth growth of the marfe into the bulk plasma.

7. Target Plate Sputtering

The sputtering of carbon at the graphite target plates was investigated by spectroscopic observation of C-lines and D_α parallel and perpendicular to the surface of the outer target plate and electron temperatures measured with a movable Langmuir probe [8]. Comparison of the carbon flux measured by a C^+-line to the D°-flux in phase I (see Sect. 6) showed a sputtering yield of about 2 % at the strike zone (see Fig. 9). By using the electron temperature to determine the incident ion energies physical sputtering yields of about 4 % were calculated. This is consistent with the

measurement if it is assumed that 50 % of the C^+ ions are swept back to the target plate.

When the divertor is cold (phase II) C^+-flux can still be observed when viewing perpendicularly to the surface, but the system viewing parallel to the surface shows very much reduced intensity. Because T_e at the target is below 5 eV during this phase this residual C^+-flux cannot arise from physical sputtering but may possibly be produced by chemical erosion of the graphite.

8. Hydrocarbons

A mass spectroscopic analysis of the exhaust gas during the discharges showed high amounts of hydrocarbons such as methane and even ethane and propane [14]. Production of 6 % carbon atoms in relation to deuterium atoms on the hydrocarbons producing surfaces could be estimated. At the same time spectroscopic observations of the inner heat shield [15] showed high carbon fluxes of the order of 2 to 10 · $10^{18}/m^2$ s. These fluxes are considerably reduced in the case of helium discharges and do not drop if the separatrix is even 10 cm away from the surfaces. An estimate attributes only a small fraction of that flux to physical sputtering. Furthermore the molecule band of the CD radical could be observed. The recalculation [24] of carbon flux born as CD_4 agrees quite well with the flux measured as C^{2+} (see Fig. 10). The increase of flux in the lower part seems to result from the inner target plate recycling. The observed fluxes of carbon correspond to a production rate of about 1.5 % C- per D-atom.

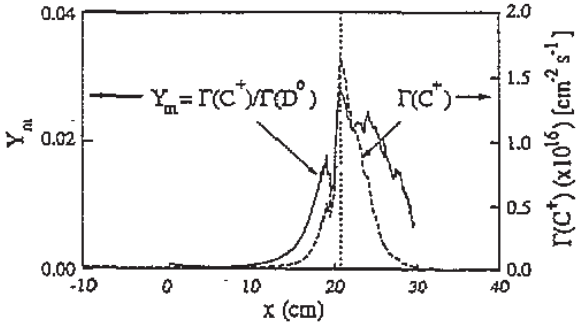

Fig. 9 Target plate sputtering

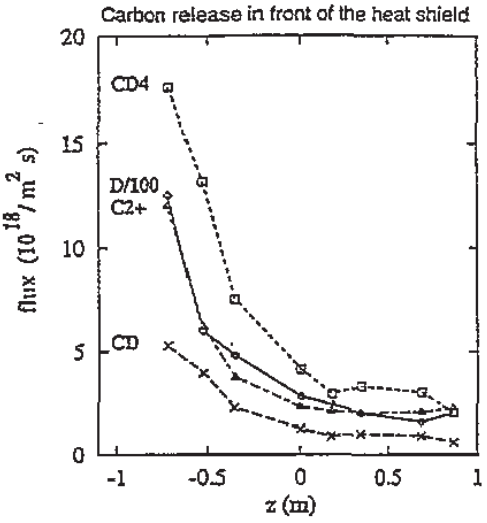

Fig. 10 Spatial profiles of CD_4 dissociations (recalculated from CD emission) and C^{2+} influx from C^{2+} line emission; z is the vertical position of measurement in front of the inner heat shield

Chemical erosion is expected to have a weak dependence on the energy of the striking particles. Together with the observation (see Sect. 6) that at the transition to a cold divertor no significant reduction of P_{rad} and Z_{eff} occurs, it can be concluded that hydrocarbon production and carbon flux from these products play a leading role for the bulk plasma impurities. The observation of carbon lines during phase

II at some distance from the target plates (see Sect. 7) seems to originate from the same process.

9. Asymmetries and Drifts

All observations described so far have been for a $\vec{B} \times \nabla$ B-drift of the ions to the X-point ($\rightarrow \times$). There are several remarkable differences if one changes to $\leftarrow \times$ operation:
1.) Reduction of the density limit by about 30 % at high q_{95}. This corresponds to a shortening of phase II, while the transition phase I/II stays nearly unchanged. 2.) H-mode could not be observed so far. 3.) The ratio of power flowing to the outer target plate to that going to the inner plate, P_{out}/P_{in}, changes from ≈ 2 to ≈ 1.4, as measured during phase I. (in phase II the thermographic system is disturbed by the Marfe radiation). 4.) During phase II an increase of the carbon fluxes by a factor of about 2 compared to the values in Fig. 10 is observed.

One would expect the case with a more balanced distribution of power to lead to a higher density limit. But one has to keep in mind that this can only be proved for phase I. In phase II no significant power flow to the target plates could be detected. The lower density limit is therefore most probably caused by a higher impurity inflow. This is in agreement with the theoretical limit for thermal instability [16] depending strongly on impurities.

A tentative explanation for the change of power flux during phase I could be the diamagnetic energy flux $\vec{q} \propto \vec{B} \times \nabla_r T$. If the radial ion temperature gradient $\nabla_r T_i$ is steeper than $\nabla_r T_e$ as observed in ASDEX, this would explain the observed effect. The increased influx of carbon on the lower inner heat shield in phase II could be attributed, on the other hand, to the poloidal temperature gradient $\nabla_p T$ and corresponding neoclassical drifts $\Gamma \propto \vec{B} \times \nabla_p T$ [17].

10. High-Z Investigation

As a first high-Z investigation tungsten samples were positioned at the target plates and their erosion and redeposition were observed [18]. After 80 discharges the samples were taken out and the tungsten deposition was measured. The surprising result showed tungsten only at short distances around the samples (see Fig. 11) while a fluid code calculation taking into account free-streaming neutrals and back-sweeping of ions by the plasma streaming to the target plates should have given a deposition pattern at a distance of about 20 mm. The effect can be attributed to a speciality of high-Z material, viz the ionization length is normally much smaller than the ion gyroradius. The major fraction (90 % calculated) should therefore return after one gyro half-cycle, in good agreement with observations.

11. Summary

The first extended period of plasma boundary investigation on ASDEX Upgrade showed a low L/H power threshold and a high density limit. Details of the power flowing through ELMs to the target plates were detected and the "dithering cycle" was identified as a general phenomenon for the transition from L to H. The density limit approach showed distinct transitions: the first transition to a cold divertor is relatively insensitive to impurities, while the second, which is characterized by a Marfe growing into the bulk plasma, depends on conditioning and impurities. The observation of carbon sources from sputtering as well as from chemical erosion proved the latter to be dominant. Characteristic differences before and after the divertor gets cold may be explained by classical drifts. High-Z investigations of target erosions showed pronounced effects of very local redeposition.

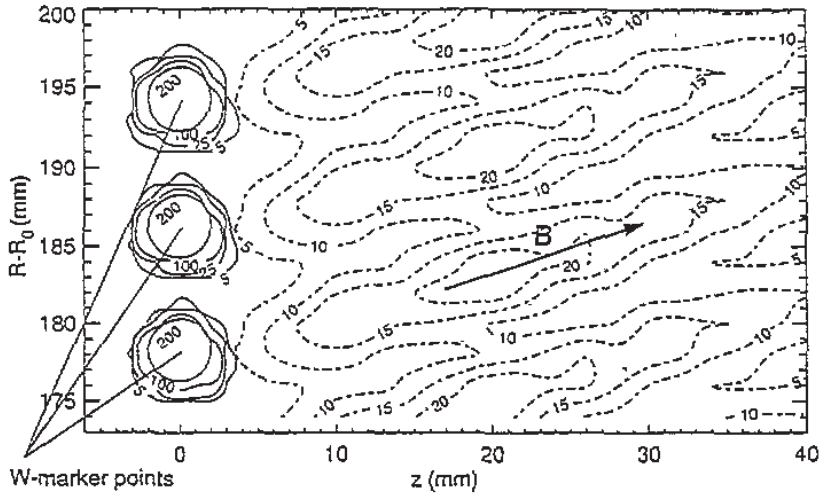

Fig. 11 Tungsten redeposition (solid lines: measured tungsten density levels; dashed lines: fluid calculations)

References

[1] W. Köppendörfer et al., 14th Intern. Conf. Plasma Phys. Contr. Fus., Würzburg, 1992;
[2] O.J.W.F. Kardaun et al., 14th IAEA Conf. Plasma Phys. Contr. Fus. CN-56/IF/1/3 (1992);
[3] A. Silva et al., Proc. 20th Europ. Conf. Contr. Fus. and Plasma Phys., 17C, III, 1107 Lisboa (1993);
[4] A. Herrmann et al., Proc. 10th Europ. Conf. Contr. Fus. and Plasma Phys., 17C, II, 567, Lisboa (1993)
[5] H. Zohm et al., Proc. 20th Europ. Conf. Contr. Fus. and Plasma Phys., 17C, I, 19, Lisboa (1993)
[6] T.E. Stringer, JET Report P(93)07;
[7] R. Schneider et al., Contr. Plasma Phys. 32 (1992), 450;
[8] C.S. Pitcher, Proc. 20th Europ. Conf. Contr. Fus. and Plasma Phys., 17C, I, 291, Lisboa (1993)
[9] H.-S. Bosch, Proc. 20th Europ. Conf. Contr. Fus. and Plasma Phys., 17C, II, 795, Lisboa (1993)
[10] J. Neuhauser et al., Plasma Physics and Contr. Fusion, Vol. 31, No. 10, p. 1551, 1989
[11] K. McCormick, Proc. 20th Europ. Conf. Contr. Fus. and Plasma Phys., 17C, II, 587, Lisboa (1993)
[12] M. Laux et al., Poster at EPS 1993, Lisboa
[13] A.R. Field, Verh. DPG (1993) P.9.3, 88;
[14] W. Poschenrieder et al., Proc. 20th Conf. Contr. Fus. and Plasma Phys., 17C,II, 591, Lisboa (1993)
[15] A. Kallenbach et al., Proc. 20th Europ. Conf. Contr. Fus. and Plasma Phys., 17C, II, 571, Lisboa (1993)
[16] J. Neuhauser et al., Nucl. Fus., vol. 26, 12 (1986);
[17] K. Lackner, A. Nocentini, Proc. of the 2 Symp. on Plasma Dynamics: Theory & Applications, Trieste (1992);
[18] D. Naujoks et al., Proc. 20th Europ. Conf. Contr. Fus. and Plasma Phys., 17C, II, 651, Lisboa (1993)

[19] V. Mertens et al., Proc. 20th Europ. Conf. Contr. Fus. and Plasma Phys., 17C, I, 267, Lisboa (1993)
[20] F. Ryter et al., Proc. 20th Europ. Conf. Contr. Fus. and Plasma Phys., 17C, I, 23, Lisboa (1993)
[21] J.-M. Noterdaeme et al., Proc. 20th Europ. Conf. Contr. Fus. and Plasma Phys., 17C, III, 945, Lisboa (1993)
[22] G. Lieder et al., Proc. 20th Europ. Conf. Contr. Fus. and Plasma Phys., 17C, II, 579, Lisboa (1993)
[23] J.-M. Noterdaeme et al., 10th Top.Conf. on RF-power in plasmas, Boston (1993)
[24] K. Behringer, J.Nucl.Mat. 176 & 177 (1990), 606